Egypt. J. Chem. **Vol. 64,** No. 2 pp. 739 - 750 (2021)

Egyptian Journal of Chemistry

http://ejchem.journals.ekb.eg/

Synthesis, Optical, and Fluorescence Properties of Mn-doped ZnS Quantum Dots

E.M. Kamar, K.A. Soliman, U.W. Tash*, S.M. Reda, M.A. Mousa

Chemistry Department, Faculty of Science, Benha University, Benha (Postcode: 13518), Egypt

Abstract

ZnS and 3 at% Mn:ZnS QDs were prepared by the hydrothermal method. The samples were characterized by XRD, FT-IR, SEM, TEM, EDX, UV-Vis spectroscopy, and photoluminescence (PL). The UV-Vis spectroscopy data showed that the peaks of the prepared ZnS and Mn:ZnS samples display a hypsochromic shift compared to that of the bulk ZnS. The calculated band-gap energy values of the ZnS and Mn:ZnS QDs are found to be 4.85 and 4.3 eV, respectively, and larger than that of bulk ZnS (3.68 eV) owing to strong quantum confinement. The calculated particle sizes from bandgap energies are found to be 1.8 nm and 1.7 nm for ZnS and Mn:ZnS, respectively. The PL measurements showed that the emission intensity of ZnS QDs increased by Mn^{2+} doping. The fluorescence quantum yield (FLQY) of ZnS and 3 at% Mn:ZnS QDs is found to be 0.86 and 0.85, respectively. The incident photon-to-electron conversion efficiency (IPCE) measurement was performed to investigate the photovoltaic properties of ZnS and 3 at% Mn: ZnS QDs. At 370 nm, the measured IPCE (%) values are found to be 1.2% and 2.1% for ZnS and Mn:ZnS, respectively, suggesting that the Mn^{2+} dopant enhances the optical properties of the host crystal (ZnS QDs).

Keywords: Quantum dots; ZnS; Mn:ZnS; IPCE (%)

1. Introduction

In recent decades, much research attention has concentrated on electronic materials made of quantum dots (QDs), which are small crystals of semiconducting materials, whose size range from 2 nm to 10 nm. Their extremely small size makes their optical and electronic properties different from those of bulk materials. A greater part of QDs can emit light of specific wavelengths if excited by light or electricity. Several publications have reported that the electronic characteristics of QDs are determined by their size and shape, which means we can control their emission wavelengths by tuning their sizes [1-4]. In the present time, scientists and researchers have shown great attention in the QDs materials as it shows broad and continuous absorption spectra in presence of white light whereas the few nanoseconds delayed emission occur at different wavelength region, which is a characteristic of the material used [1,2]. The fluorescent researches point that the emission frequencies increase as the size of the quantum dot decreases, causing a blue shift in the electromagnetic spectra. Their greatly tunable optical properties based on their size are attractive, directing to a collection of research and commercial applications, including solar cells, transistors, LEDs, medical imaging, and quantum computing [3,4].

Silicon-based solar cells are presently the furthermost common type of solar cell used. However, silicon solar cells have low spectral sensitivity to ultraviolet light. To resolve this drawback, the improvement of a wavelength conversion material that switches light in the ultraviolet wavelength region to visible light at the high spectral sensitivity of a silicon-based solar cell is requested.[5] Recently, the application of organic dyes and semiconductor quantum dots (QDs) [6] as wavelength conversion materials has drawn much consideration. However, the use of organic dyes as a

*Corresponding author e-mail: osama.tash@fsc.bu.edu.eg
Receive Date: 26 August 2020, Revise Date: 16 September 2020, Accept Date: 27 September 2020
DOI: 10.21608/EJCHEM.2020.40626.2824

wavelength conversion material is limited because they can only absorb light in a limited wavelength range corresponding to their intrinsic absorption characteristics [7]. On the other hand, semiconductor QDs can absorb light in all wavelength regions shorter than their absorption onset and it is possible to control the onset wavelength via the QD size due to quantum size effects.[8] Moreover, when compared to organic dyes, QDs are more stable against light irradiation.[7] Thus, it is believed that they have great potential as a wavelength conversion material.

The synthesis of quantum dots can succeed mainly by two approaches: a top- down and a bottom-up method [9,10]. The top-down processes include several techniques such as electron beam lithography, focused ion beam (FIB), and etching; these fabrication processes suffer from structural defects and incorporation of various impurities during its long synthetic pathways. The second kind of the synthetic process is the bottom-up method, which consists of two types a) wet-chemical and b) vapor-phase methods. The wet-chemical method deals with reactions in the solution phase such as the sol-gel process, microemulsion, hot-solution decomposition, etc; whereas, in the vapor-phase method, molecular beam epitaxy (MBE), sputtering, liquid metal ion sources, physical or chemical vapor deposition are more important. Generally, the most common routes to prepare pure nanomaterials are the bottom-up methods.

II-VI semiconductors are well known as QDs with size-tunable absorption and emission. Unfortunately, the QDs of these semiconductors have been up to now made up of toxic compounds (Cd, Pb, Hg, Te, As, etc.) [11]. On the other hand, ZnS dots exhibit lower cytotoxicity, higher excited state lifetimes, and greater thermal and environmental stability [12]. Therefore, ZnS can be applied to photovoltaic uses since it has the band gaps 3.8 eV and 3.66 eV for the bulk hexagonal and cubic structures, respectively [13]. The incorporation of transition-metal dopants such as Cu and Co ions initiates intermediate energy states, like trap states, between the valence and the conduction bands of host semiconductor nanocrystals and manipulates the relaxation dynamics of host materials [14-17]. Consequently, the dopant emission causes unique optical properties whose nature changes with selected hosts and dopants. The Mn^{2+} ion is considered as an ideal dopant because it can deliver a luminescent center and can also show hyperfine splitting in electron paramagnetic resonance spectra [18]. The Mn^{2+} dopant acts as emissive traps because the trapped energy levels are arranged between the valence and conduction bands of the host crystal [19]. Accordingly, the trap statuses modify the optical and electronic properties of the host. It is broadly assumed that the excitation occurs through the host lattice and is followed by energy transfer to the impurity to produce the Mn luminescence band in Mn^{2+}- doped ZnS quantum dots. Moreover, it was found that the luminescence properties of Mn:ZnS QDs synthesized by various procedures have a good correlation with the synthetic conditions [20-23].

Based on the mentioned above, in the present work, we synthesized Mn^{2+}-doped ZnS QDs with excellent optical and fluorescence properties using a hydrothermal method to produce QDs with narrow size distribution, high quantum yields, effectively lower reaction time and smaller amount of surface defects [24]. The structure, photoluminescence, and optical properties of the synthesized samples were investigated.

2. Experimental

2.1. Materials

Zinc acetate dihydrate ($Zn(CH_3COO)_2{\cdot}2H_2O$) and Manganese acetate tetrahydrate ($Mn(CH_3COO)_2.4H_2O$) were purchased from LOBA Chemie. Thiourea (NH_2CSNH_2) and Acetone were supplied from ADWIC. All the precursors are commercially available and have high purity (no further purification was carried out).

2.2. Preparation methods

2.2.1. Preparation of ZnS QDs:

The ZnS quantum dots solid was prepared by a simple chemical route, where 25 mL of 0.25 M zinc acetate solution, prepared 3 hours before being used, was added dropwise to a freshly prepared 25-mL solution of 0.75 M thiourea. The mixed solution was stirred for 30 minutes before pouring into a Teflon-lined autoclave with a capacity of 50 mL and then putting it at 200 °C in a furnace for 24 hours. The reaction was eventually quenched by cooling down to

room temperature so that the precipitated product can cool down. The obtained white precipitate was washed several times with double-distilled water and acetone, respectively, and finally dried for 12 hours at 100 ◦C and stored in an airtight container for characterization [25**].**

2.2.2. Preparation of Mn-doped ZnS QDs (3 at% Mn:ZnS QDs)

3 at% Manganese-doped ZnS QDs were also synthesized by the hydrothermal method, where 12.5 mL (0.25 M) Manganese acetate solution was added to 12.5 mL (0.25 M) Zinc acetate solution dropwise with continuous stirring. The mixed solution was added to a 25-mL solution of thiourea (0.75 M) drop by drop. Then, the mixed solution was stirred for 30 minutes, followed by pouring into a sealed Teflon-lined autoclave with a capacity of 50 mL, which was finally placed at 200 ◦C in an oven for 24 hours. After applying the heat, we moved the autoclave out of the oven so that the precipitated product can cool down. The obtained pink precipitate was purified with deionized water, washed with acetone, and finally dried for 12 hours at 100 ◦C. Then, it was stored in an airtight container for characterization [25].

2.3. The incident photon-to-electron conversion efficiency (IPCE)

IPCE of QDs [26] was evaluated using the Perkin Elmer Lamda-900 spectrophotometer. The as-prepared samples served as a photoanode. Electrodes were prepared by mixing the as-prepared QDs with few drops of ethanol to get a slurry form, then, it was assembled on FTO and dried at 30 °C for one hour to vaporize the solvent and achieve the best adhesion on the surface of the substrate. The counter electrode was organized by sputtering a thin layer of carbon over a transparent conducting glass (TCO glass layer, transmission > 70% with sheet resistance = 20 Ω/square) using a graphite rod. The electrolyte was formulated by mixing 0.02 M of I_2 and KI as a redox couple in acetonitrile. The photoanode was then joined to the carbon counter electrode and the edges of the cell were sealed. The electrolyte was introduced by a syringe into the space between the two electrodes. IPCE was measured immediately after device fabrication. The current was carried out using an electrometer (model 6517, Keithley).

2.4. Characterization techniques

XRD analysis was performed by using Bruker Advance D8 Ew, Germany with Cu Kα radiation with a wavelength value of 1.54178 Å. The Fourier transform infrared (FT-IR) spectra of the samples were documented in the range 4000–400 cm^{-1} with 2 cm^{-1} resolution using a double beam Perkin Elmer Spectrometer. Scanning Double-beam UV–Vis spectrometer Lambda 950 (PerkinElmer), in the range of 200-800 nm, was used for measuring the optical absorbance at room temperature. The fluorescence spectra of the studied samples were recorded with the FluoroSENS-9000 photoluminescence spectrophotometer provided by a 150-Watt xenon lamp as an excitation source with a laser wavelength of 440 nm. The quantum yield (QY) was calculated comparative to a fluorescein reference solution. The size and morphology of the Mn:ZnS sample was determined by using TEM (JEOL JEM-2100) and scanning electron microscopy (SEM, Zeiss Sigma 300 PV, Germany). Elemental analysis was carried out by energy dispersion spectroscopy (EDX).

2.5. Computational Details

The 3 ϰ 3 ϰ 3 supercells for ZnS and Mn^{2+} doped ZnS crystal calculations were done by using $DMol^3$ code in Materials Studio 2017 software [27, 28]. The Double numeric polarized (DND) version 4.4 basis sets with Perdew-Burkle-Ernzerhof (PBE) forms of generalized gradient approximation (GGA) to the exchange-correction interaction was used [29]. The effective core potentials with density mixing fraction 0.2 and direct inversion in the iterative subspace (DIIS size 6) and orbital occupancy with a smearing of 0.005 Ha were employed. The orbital cutoff distance was set at 4.4 Å for all atoms. The DFT-D correction of the Grimme method was applied with an *s6* factor of 0.75 and a damping factor *d* of 20.0. The density of states (DOS) and partial density of states (PDOS) were calculated with 1 empty band and a *k*-point grid of 2 × 2 × 2.

3. Results and discussion

3.1. Structure characterization of ZnS and Mn-doped ZnS (Mn: ZnS) QDs

3.1.1. Fourier Transform Infrared Spectroscopy Results

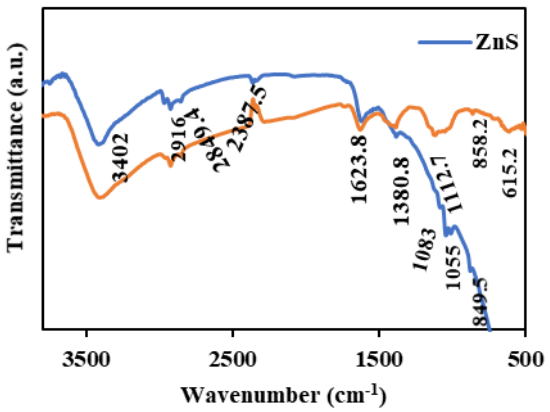

Fig. 1. FTIR spectra of ZnS and Mn:ZnS QDs.

Fig. 1 represents the FTIR spectra of the investigated ZnS and Mn:ZnS QDs. The spectra of both samples showed a band at 1380 cm^{-1}, assigned to the symmetric stretching vibration mode of carboxylate (COO^-) group [30], indicating the presence of the acetate group after the preparation of the samples. The band appearing at 3380 cm^{-1} may be due to H_2O stretching, since H_2O is adsorbed on the surface of the particles [31]. The band around 1620 cm^{-1} is attributed to the bending mode of the hydroxyl group (O-H) [31]. All the mentioned bands are detected in all the studied samples. The peak situated around 1040 cm^{-1} is assigned to the stretching of S–O, and the one that appears at 840 cm^{-1} is characteristic of the ZnS stretching vibration [30]**.** The peaks at 610 cm^{-1} are assigned to symmetric bending of Zn-S and Mn-S [32]. On comparing the FTIR spectra of ZnS and Mn:ZnS QDs, the weak band appearing at 2370 cm^{-1} for ZnS, corresponding to C=O stretching vibrations, has completely disappeared upon doping ZnS with Mn^{2+} [32]. In the spectrum of Mn:ZnS, the band observed at around 1110 cm^{-1} is assigned to symmetric stretching modes of the ions under investigation [32].

3.1.2. X-ray diffraction (XRD)

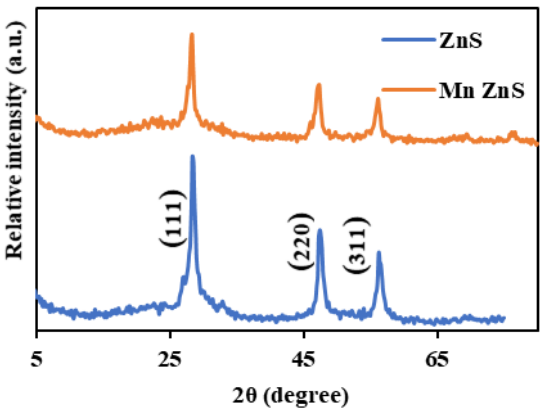

Fig. 2. XRD patterns of ZnS and Mn:ZnS QDs.

Fig. 2 represents the X-ray diffraction (XRD) patterns of the ZnS and Mn:ZnS QDs samples. All the quantum dots' peaks match the cubic structure of ZnS, JCPDS card, no. 05-0566. The 3 XRD peaks (at $2\theta = 28.48^\circ$, 47.52° , and 56.32°) correspond to the following planes: (111), (220) and (311) [32]. The broadened peaks indicate the small particle sizes of the samples [34]. The diffraction peaks observed in Mn:ZnS sample refer to the fact that doping of ZnS with Mn^{2+} ions leads to Mn^{2+} separation [35]. Moreover, the nonexistence of extra impurity phases in Mn:ZnS QDs proves that doping has been carried out successfully [33].

The Debye-Scherrer's formula [33] was used to estimate the crystal sizes of ZnS and Mn:ZnS QDs.

$$D = \frac{0.9\lambda}{\beta\cos\theta} \quad (1)$$

where D is the average size of the crystal, λ (= 1.5406 Å) is the wavelength of the Cu $K_{\alpha 1}$ X-rays, β is the full width at half-maximum (FWHM), and θ is the Bragg diffraction angle [33]. The crystallite size was evaluated from the broadening of the (111) plane and found to be 4.9 and 3 nm for ZnS and Mn:ZnS, respectively. The reduction of crystal size for Mn:ZnS can be attributed to small grain growth of Mn^{2+} compared to Mn-free ZnS QDs [35]. The obtained particle size is smaller than the Bohr radius of ZnS [36]. These results prove that the quantum dots (QDs) were successfully prepared.

The lattice constant values 'a' of ZnS and Mn:ZnS QDs were calculated using the following relation [33]:

$$\frac{1}{d_{hkl}^2} = \frac{h^2+k^2+l^2}{a^2} \quad (2)$$

Where d is the d-spacing of the plane (111) and (hkl) are the Miller indices. The a- value is found to be 5.4 and 5.42 Å for Mn^{2+}-free ZnS and Mn^{2+}-doped ZnS, respectively. The slight increase in "a" value for Mn:ZnS could be attributed to the incorporation of Mn^{2+} dopant into the zinc matrix because the radius of Mn^{2+} ions (0.80 Å) is larger than that of Zn^{2+} ions (0.74 Å) [37].

The dislocation density δ, i.e. the parameter that represents a sample's defects, was calculated by the following equation [34]:

$$\delta = 1/D^2 \quad (3)$$

where D is the average size of the crystal. The value of δ for ZnS and Mn: ZnS was found to be 1.11 $x10^{17}$ and $3.3x10^{16}$ lines/m^2, respectively.

The strain is also calculated for both ZnS and Mn:ZnS QDs using the following equation [34]:

$$\text{Average strain} = \frac{\beta\ (in\ radians)}{4\ tan\theta} \quad (4)$$

where $\beta = \frac{0.9 \times \lambda}{crystal\ size \times cos\theta}$ and λ= 0.154 nm. It was found that the Strain of ZnS and Mn: ZnS is 2.5 x 10^{-4} and 3.6x 10^{-4}, respectively.

3.1.3. SEM and TEM characterization

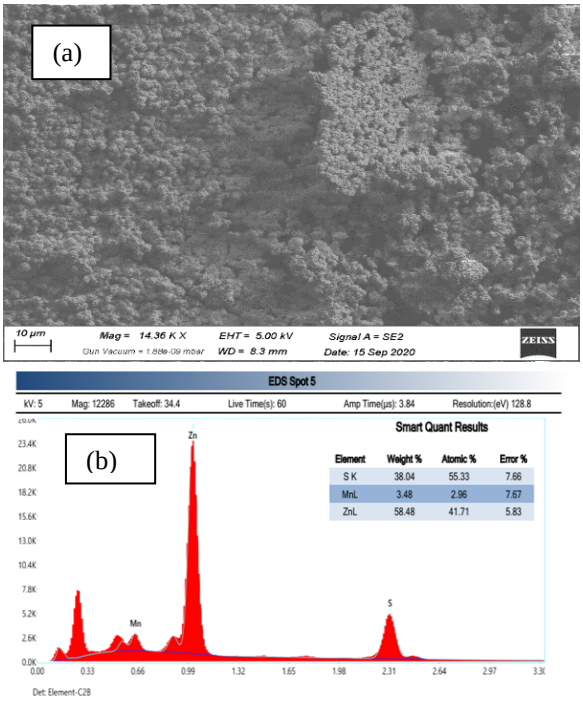

Fig. 3. SEM image of Mn:ZnS (a), and EDX analysis (b).

The morphology of the Mn:ZnS was observed by SEM and TEM images. Fig. 3 shows the SEM images of synthesized Mn^{2+}-doped ZnS nanoparticles. These nanoparticles are nearly spherical in shape. The elemental composition determined through EDX attached with SEM instrument is shown Fig. 3(b). This reveals that the Mn^{2+} ions are incorporated with ~ 3 at% in the ZnS lattice. The TEM micrographs of Fig. 4 confirm the crystallinity and the small dimension of Mn:ZnS NPs with an average size of 4.3 nm.

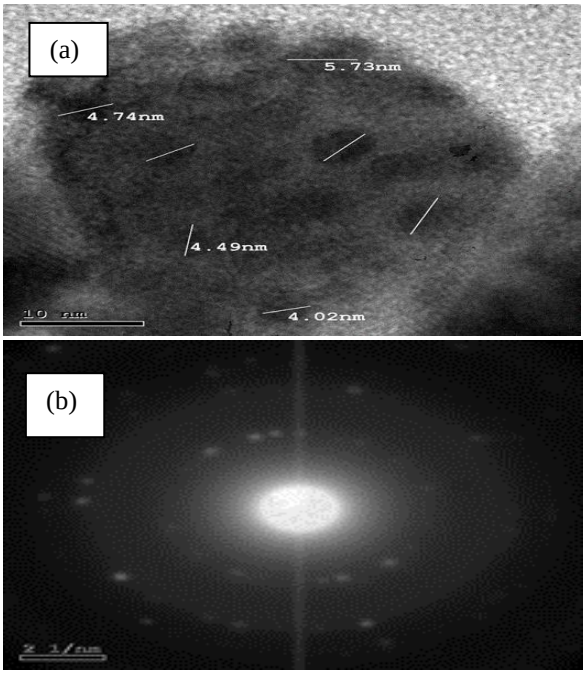

Fig. 4. TEM micrograph of Mn:ZnS nanoparticles including TEM-image (**a**), and SAED (b).

3.2. Optical Characterization

3.2.1. UV-Visible Absorption

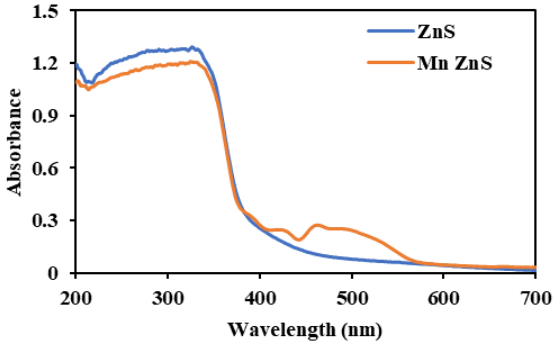

Fig. 5. UV-Vis absorption spectra of ZnS and Mn: ZnS QDs.

Fig. 5 demonstrates the UV-Visible spectra of ZnS and Mn:ZnS QDs in the range of 200-800 nm. The spectra of the samples represent the electronic transition from the valence band to the conduction band [38]. The QDs' absorption edges (λ_o) of the studied samples were blue-shifted from 345 nm [39] (the bulk's value of ZnS) to 325 nm. This shift is assigned to the quantum confinement of the samples, which leads to a more distinct energy spectrum of the singular QDs. The quantum confinement effect on the impurity depends upon the size of the host crystal. That is, the extent of confinement increases when the size of the host crystal reduces [39]. The observed optical absorption at 325 nm represents the $S_{3/2}$ (h)-to-1S (e) first excited electronic transition [40].

3.2.2. Bandgap determination

The bandgaps, i.e. the gap between valence and conduction bands, of our QDs were calculated from the UV-Visible spectra using the following equation [25]:.

$$(\alpha h\nu) = K(h\nu - E_g)^{n/2} \quad (5)$$

Where α *is the* absorption coefficient, h is Planck's constant, ν is the light frequency, K is constant, E_g is the bandgap, and n is a constant (= 1 for direct band gaps). The α value was calculated from the optical absorbance (A) and the film thickness (t) using the following equation [41]:

$$\alpha = 2.3026\,A/t \quad (6)$$

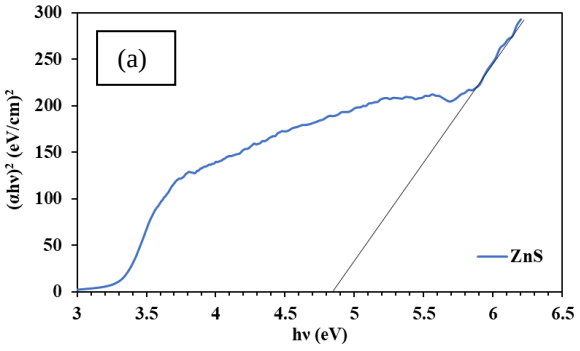

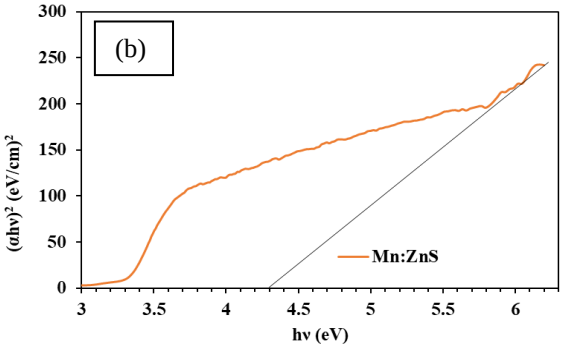

Fig. 6. Plots of $(\alpha h\nu)^2$ versus energy band gap (E_g) of (a) ZnS and (b) Mn: ZnS QDs.

The plots of $(\alpha h\nu)^2$ vs. $h\nu$, Fig. 6 (a) and 6 (b), show linear parts, confirming the predomination of the direct mode of the optical transition, and the intercept between the linear part with the X-axes determines the E_g values. These calculated band-gap values are found to be 4.85 and 4.3 eV for the Mn^{2+}-free ZnS and Mn:ZnS samples, respectively. The obtained E_g values are greater than that of bulk ZnS (3.68 eV), referring to the strong quantum confinement in the investigated samples [39]. The quantum confinement theories state that the potential barrier of the surface restricts the valence band's holes and the conduction band's electrons [41], resulting in a larger separation of the bandgaps [39].

The optical absorbance shifts to red wavelength by doping ZnS with Mn^{2+}, i.e. the energy gap decreases as shown in Fig.6 (b). This could be attributed to the fact that Mn^{2+} forms new 3d energy levels in the ZnS energy band. This change in the gap between the valence and conduction bands finds a new channel for excitation [39]. So, it can be said that the Mn^{2+} dopant increases the bandgap of ZnS compared with the undoped QDs and, accordingly, enhances the photon-to-charge output efficiency [25].

3.2.3. Particle size studies

The particle sizes of the investigated QDs could be determined from the calculated E_g values using the following Brus relation [36]:

$$E_{np} = E_g + \frac{h^2}{8r^2}\left[\frac{1}{m_e^*} + \frac{1}{m_h^*}\right] - \frac{1.8e^2}{4\pi\varepsilon_o\varepsilon_r} \quad (7)$$

where E_{np} is nano-particle bandgap, r is the QD's radius expressed in nm, m_e* is the effective mass of the electron, m_e is the mass of an electron (for ZnS,

m_e* = 0.25 m_e), m_h* is the effective mass of the hole, m_h is the mass of a hole (for ZnS m_h* = 0.60 m_e), e is the charge on the electron, ε_r is the dielectric constant of material (for ZnS, ε = 8.3), and ε_o is the vacuum permittivity constant. The quantum dot particle size ($D^/$) calculated from the value of r, where $D^/$ =2r, are found to be 1.8 and 1.7 nm for ZnS and Mn:ZnS samples, respectively. These obtained particle sizes are smaller than the Bohr exciton radius of the samples under investigation, where the Bohr radius for ZnS is 5 nm [36]. Also, the particle sizes are smaller than the crystallite sizes (D) obtained from the XRD pattern. The results match the data found in references [35, 38, 42]. The difference found between D and $D^/$ values can be attributed to the sensitivity of the XRD analysis to the crystalline size [43], whereas the solvent may affect the particle size determination from the UV-Vis spectra [44].

3.3. Photoluminescence Characteristics and Fluorescence quantum yield

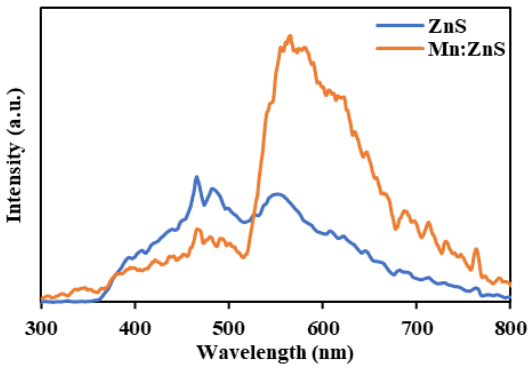

Fig. 7. Fluorescence emission spectra of ZnS and Mn: ZnS QDs.

The photoluminescence (PL) analysis was carried out at room temperature for the prepared materials. Fig. 7 represents the obtained PL spectra, which shows two different peaks for ZnS QDs located in the blue region (about 470 nm) and the yellow region (about 570 nm). The 470 nm peak can be attributed to the zinc vacancy and conduction band recombination, while the 570 nm peak may be due to the sulfur vacancy and related acceptor center recombination [13]. Zinc ions are smaller than sulfur ions, so the latter increases the strain of the lattice. Sulfur ions exist in interstitial positions close to the valence band edge, and as a result of the newly-acquired strain [13], the energy levels at the interstitial sites have small binding energy.

New levels were introduced within the bandgap on doping with Mn^{2+}, which changes the ZnS QDs' optical properties, especially the photoluminescence characteristics of the undoped ZnS QDs. As shown in Fig. 7, Mn:ZnS QDs exhibit a peak at around 570 nm, which is attributed to the transition from $^4T_1$ excited state of Mn^{2+} to the ground state of Mn^{2+} ($^6A_1$). The value is blue-shifted compared with that of bulk Mn:ZnS [38]. Large density of surface states in the nanoparticles, strong electron-phonon coupling in the nanoparticles, or size-dependent crystal field effect may be the reasons why the peaks of Mn:ZnS QDs are red-shifted [45]. From the emission spectrum of Mn:ZnS QDs, part of Mn^{2+} ions doped the ZnS crystal, and the other part stays on the surface. The intensity of photoluminescence of the Mn^{2+}-free ZnS QDs at around 470 nm (due to the S^{2-} vacancy) is not quenched in Mn:ZnS QDs whereas after doping ZnS with Mn^{2+}, the fluorescence intensity of Mn:ZnS sample at 570 nm was found to be 3 times higher than that of undoped ZnS QDs. Since the two samples were prepared under the same experimental orders, the obtained result demonstrates the presence of a strong interaction between the d-electron states of Mn^{2+} ions and the s-p states of ZnS host lattice. This, in turn, provides an effective channel for the transfer of electrons and holes, leading to the subsequent emission in ZnS:Mn^{2+} QDs [38]. The strong PL emissions indicate that the prepared QDs have large bandgaps compared with their bulk counterpart. The property that the particles emit intensive and broad yellow luminescence indicates that the ZnS and Mn:ZnS QDs would be good candidates for luminescent solar collector applications.

The fluorescence quantum yield (PLQY) defines the efficiency of the fluorescence process. The absolute fluorescence quantum yields "ϕ_f" of ZnS and Mn:ZnS QDs were investigated and computed using the following equation [46]:

$$\phi_f = \phi_{f(ref)} \, (a/a_{ref})(n/n_{ref})(A_{ref}/A) \quad (8)$$

where ϕ_{ref} is the fluorescence quantum yield of the fluorescein (excited at 460 nm) as a reference, a is the absorbance, n is the refractive index of the solvent, and A is the area under the fluorescence curve. The calculated PLQY of ZnS and Mn:ZnS QDs is found to be about 0.86 and 0.85, respectively. The high PLQY may be due to surface passivation. Surface passivation strategies, i.e. a method to fix the QDs'

fluorescence characteristics by eliminating non-radiative surface defects, confine the wave function of electrons and holes pairs to the inside of the crystals, which, in turn, decreases the non-radiative relaxation [47].

Mn^{2+} ions did not affect the PLQY of ZnS because Mn and ZnS have almost similar band gaps (3.6 and 3.1 eV), which results in the separation of the electron and hole into the core and shell individually. This allows a better adjustment of the bandgap since both the core diameter (Mn) and the shell thickness (ZnS) affect the QD electronically [47].

3.4. The incident photon to current efficiency (IPCE%) of ZnS and Mn: ZnS QDs

IPCE (%), i.e. the ability of the QDs to produce photocurrent at a specific wavelength of incident light and given by the fractional ratio of the number of electrons generated to the number of incident photons, was measured by the bombardment of different wavelengths of light. IPCE (%) is an important parameter to describe and understand the photoconversion property of the investigated QDs. It can be given by the following relation [48]:

$$\text{IPCE} = \frac{1240 \times I}{\lambda \times P_{in}} \quad (9)$$

where I is the density of current at a given wavelength, λ is the wavelength of incident light, and P_{in} is the intensity of the light at a given wavelength.

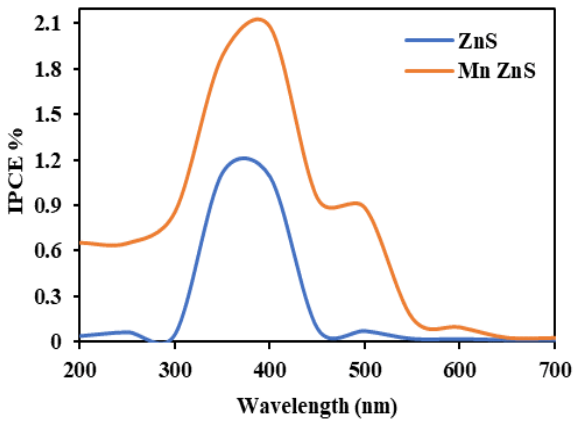

Fig. 8. IPCE% of ZnS and Mn:Zn QDs.

Fig. 8 compares the IPCE (%) measurements of ZnS and Mn:ZnS QDs. Two important observations should be considered. One of these is the enhanced IPCE (%) of Mn:ZnS QDs compared to the undoped ZnS QDs, which has been detected along the visible range. At 370 nm, the IPCE (%) values are 1.2 % and 2.1 % for ZnS and Mn:ZnS, respectively, showing that the Mn^{2+} dopant boosts the photoconversion efficiency of ZnS QDs. The Mn^{2+} ions increase the number of excited electrons and suppress the dark produced current [49], leading to a higher IPCE (%) value for Mn:ZnS QDs compared with ZnS QDs. Moreover, the spectral response range of Mn:ZnS QDs is wider than that of ZnS QDs owing to the Mn^{2+} impurities effect. The newly-introduced energy levels of Mn^{2+} to the host's conduction band is the reason why there is an increase in the spectral response range and consequently the photocurrent conversion of the QDs [49].

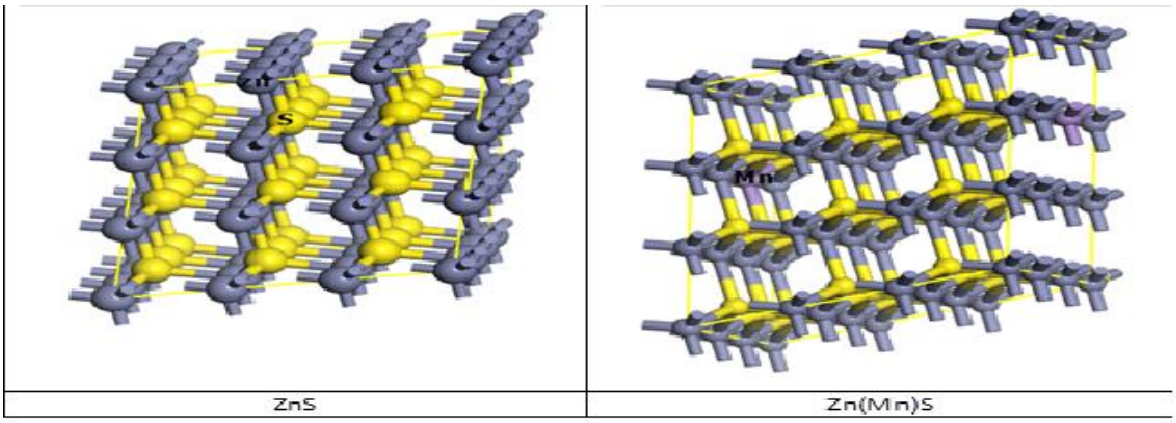

Fig 9. Optimized cell of ZnS and Mn:ZnS crystals.

3.5. Computational details of ZnS and Mn: ZnS QDs

First, we performed geometry optimization for ZnS and Mn^{2+}-doped ZnS crystal, which appeared as 3 ˣ 3 ˣ 3 supercells for calculations as shown in Fig. 9. ZnS crystallizes in a cubic system with an F-43m space group. The optimized lattice parameters of ZnS and Mn^{2+}-doped ZnS crystal were presented in Table 1. The variation of the lattice parameters with Mn^{2+} doped ZnS crystal shows a little increase of the lattice constant, as shown in XRD results. The bond length between Zn-S and Mn-S in the pure and doped cell were 2.360, 2.361, and 2.398 Å respectively. The Mulliken charge was proceeded to evaluate atomic charges as seen in Table 2. The charges of Zn and S were 0.512 (e) and -0.512 (e) in the pure cell. For Mn^{2+} doped ZnS crystal, the charges of Zn, Mn, and S were 0.557 (e), 0.263 (e), and -0.564 (e) respectively which is related to electron losses and gains.

We investigated the density of states (DOS) and the partial density of states (PDOS) to understand their electronic properties. As shown in Fig. 10, the peaks of DOS at -11.79 eV is small and mainly provides s states for S. The next peak appears at around -6.13 eV which is attributed to d states of Zn with some p states of S. The energy range of -4.40 eV and 0.60 eV of DOS arises from partially mixed p states of S with s states of Zn, and they contribute to valence edge band. Above Fermi level, the DOS mainly attributes to s and p states of Zn mixed partially with a little d states of S. By doping ZnS with Mn^{2+}, as seen in Fig. 11, the energy DOS for Mn appears in a range between -4.82 eV and 0.27 eV for d beta states and the small peak of d alpha state, but the density d alpha states of Mn appears at energy of 2.62 eV above the Fermi level. This doping process causes the Fermi level-shifted towards the valence band and the energy gap to decrease, as shown from the UV-vis absorbance data. The bandgap computed with GGA functional is underestimated. This disagreement with experimental value by ~ 46% for ZnS and 41% for Zn(Mn)S.

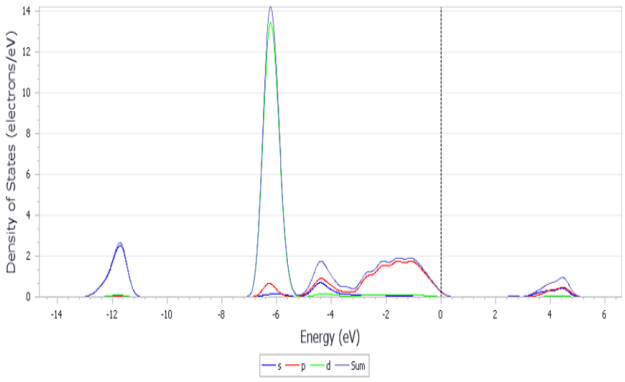

Fig. 10. DOS and PDOS of ZnS crystal.

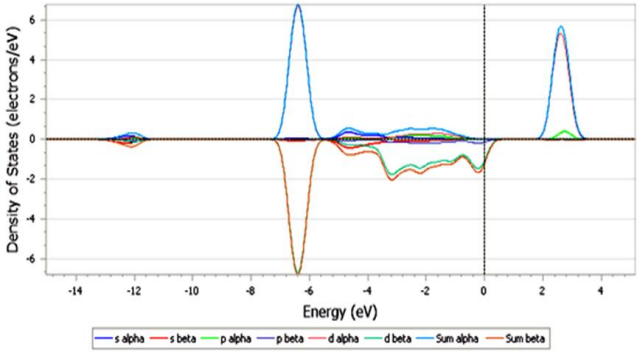

Fig. 11. DOS and PDOS of Mn:ZnS crystal.

Table 1 :Lattice parameters of ZnS and Mn:ZnS samples.

Materials	a (Å)	b (Å)	c (Å)	α	β	γ
ZnS	11.608	11.608	11.608	60	60	60
Zn(Mn)S	11.716	11.728	11.714	60	60.07	60.02

Table 2: Population analysis and energy gap results of ZnS and Mn:ZnS crystals.

Materials	Species	Charge (e)	bond	Length (Å)	Fermi energy (eV)	Energy gap (eV)
ZnS	Zn	0.512	Zn-S	2.360	-4.106	2.171
	S	-0.512				
Zn(Mn)S	Zn	0.557	Zn-S	2.361	-4.277	1.790
	S	-0.564	Mn-S	2.398		
	Mn	0.263				

4.Conclusions

In this work, ZnS, and Mn (3 at%):ZnS QDs have been investigated for QD LSCs. ZnS and Mn:ZnS QDs were successfully synthesized via hydrothermal method.

The XRD patterns indicated that the two quantum dots have a cubic crystal structure. The crystallite size for ZnS and Mn:ZnS was 4.9 and 3 nm, respectively, as calculated by the Scherrer equation. UV-Vis absorption spectra showed a blue shift for both ZnS and Mn:ZnS QDs compared with bulk ZnS due to the quantum confinement effect. The bandgap values (4.5 and 4.3 eV) of ZnS and Mn:ZnS QDs were found to be greater than the bandgap value (3.68 eV) of bulk ZnS. The intensity of fluorescence peaking around 570 nm for Mn:ZnS QDs magnifies threefold compared to the Mn^{2+}-free ZnS QDs. At 470 nm, a broad PL peak was noticed for both QDs. The PL results refer to an interaction occurring between the Mn^{2+} ions' d-electron states and the ZnS lattice's s-p states, providing a better path for the electrons-holes transfer.

PLQY of ZnS and Mn: ZnS QDs were calculated to be about 0.86 and 0.85, respectively. The high PLQY may be due to surface passivation. The properties that the particles emit intensive and broad yellow luminescence indicates that the ZnS and Mn:ZnS QDs would be suitable materials for luminescent solar collector applications. At 370 nm, the IPCE (%) values are 1.2 % and 2.1 % for ZnS and Mn:ZnS, respectively, showing that the Mn^{2+} dopant boosts the photoconversion efficiency of ZnS QDs. The Mn^{2+} ions increase the number of excited electrons and suppress the dark produced current, leading to a higher IPCE (%) value for Mn:ZnS QDs compared with ZnS QDs.

5.Conflicts of interest

There are no conflicts to declare.

6. Acknowledgements

We thank the anonymous referees for their invaluable suggestions.

7.References

[1] P. Deb, A. Bhattacharyya, S. K. Ghosh, R. Ray, and A. Lahiri "Excellent biocompatibility of semiconductor quantum dots encased in multifunctional poly(Nisopropylacrylamide nanoreservoirs and nuclear specific labeling of growing neurons," *Appl. Phys. Lett*., vol. 98, pp. 103702–103703, 2011.

[2] R. Bakalova, H Ohba, and Z. Zhelev, "Quantum dots as photosensitizers," *Nat. Biotechnol.*, vol. 22, pp. 1360-1361, 2004.

[3] R. Subha, V. Nalla, J. H. Yu et al., "Efficient photoluminescence of Mn^{2+}-doped ZnS quantum dots excited by two-photon absorption in near-infrared window II," *J. Phys. Chem. C*, vol. 117, no. 40, pp. 20905–20911, 2013.

[4] W. Zhang, Y. Li, H. Zhang, X. Zhou, and X. Zhong, "Facile synthesis of highly luminescent Mn-doped ZnS nanocrystals," *Inorg. Chem.*, vol. 50, no. 20, pp. 10432–10438, 2011.

[5] L. Danos, T. Parel, T. Markvart, V. Barrioz, W. S. M. Brooks, and S. J. C. Irvine, "Increased efficiencies on CdTe solar cells via luminescence down-shifting with excitation energy transfer between dyes," *Solar Energy Mater. and Solar Cells*, vol. 98, pp. 486-490, 2012.

[6] S.W. Beak, J.-H. Shim, and J.-G. Park," The energy-down-shift effect of Cd(0.5)Zn(0.5)S-ZnS core-shell quantum dots on power-conversion-efficiency enhancement in silicon solar cells, Phys. Chem. Chem. Phys., vol. 16, pp. 18205, 2014.

[7] J. Zhou, Y. Yang, and C.-Y. Zhang, **"**Toward Biocompatible Semiconductor Quantum Dots: From Biosynthesis and Bioconjugation to Biomedicaln Application," *Chem. Rev.*, vol. 115, pp. 11669, 2015.

[8] L. Brus, "Quantum crystallites and nonlinear optics," *Appl. Phys. A***,** vol. 53, pp. 465-474, 1991.

[9] R. Karmakar, "*Quantum Dots and it method of preparations – revisited,"* Prajnan O Sadhona, vol. 2, pp. 116-142, 2015.

[10] B. Chen, D. Li, and F. Wang, *InP quantum dots: synthesis and lighting applications*, small, vol. 16, pp. 20200245, 2020.

[11] Y. B. Wang, X. H. Liang, X. Ma et al., "Simple and greener synthesis of highly photoluminescence Mn^{2+}-doped ZnS quantum dots and its surface passivation mechanism," *Applied Surface Science*, vol. 316, pp. 54–61, 2014.

[12] O. Kolmykov, J. Coulon, J. Lalevee, H. Alem, G. Medjahdi, ´ and R. Schneider, "Aqueous synthesis of highly luminescent glutathione-capped Mn^{2+}-doped ZnS quantum dots," Materials Science and Engineering C, vol. 44, pp. 17–23, 2014.

[13] B. Bodo and R. Singha, "Structural and Optical Properties of ZnS Quantum synthesized by

CBD method," *Int. J. Sci. Res. Publ.*, vol. 6, no. 8, pp. 461–465, 2016.

[14] X. Yuan, J. Zheng, R. Zeng, P. Jing, W. Ji, J. Zhao, W. Yang, and H. Li, "Thermal stability of Mn^{2+} ion luminescence in Mn-doped core-shell quantum Dots," *Nanoscale*, vol. 6, pp. 300–307, 2014.

[15] C. Chen, P. Zhang, G. Gao, D. Gao, Y. Yang, H. Liu, Y. Wang, P. Gong, and L. Cai, (2014) Near-infrared-emitting two-dimensional codes based on lattice strained core/(doped) shell quantum dots with long fluorescence lifetime," *Adv Mater*, vol. 26, pp. 6313–6317, 2014.

[16] L. C. de S Viol, E. Raphael, J. Bettini, J. L. Ferrari, and M. A. Schiavon, "A simple strategy to prepare colloidal Cu-doped ZnSe(S) green emitter nanocrystals inaqueous media," Part. Part Syst. Char., vol. 31, pp. 1084–1090, 2014.

[17] K. E. Knowles, K. H. Hartstein, T. B. Kilburn, A. Marchioro, H. D. Nelson, P. J. Whitham, and D. R. Gamelin, "Luminescent colloidal semiconductor nanocrystals containing copper: synthesis, photophysics, and applications," *Chem. Rev,"* vol. 116, pp. 10820–10851, 2016.

[18] P. A. G. Beermann, B. R. McGarvey, S. Muralidharan, and R. C. W. Sung, "EPR spectra of Mn^{2+}-doped ZnS quantum dots," *Chemistry of Materials*, vol. 16, no. 5,pp. 915–918, 2004.

[19] B. B. Srivastava, S. Jana, N. S. Karan et al., "Highly luminescent Mn-doped ZnS nanocrystals: gram-scale synthesis," *The Journal of Physical Chemistry Letters*, vol. 1, no. 9, pp. 1454–1458, 2010.

[20] S. Kumar, H. C. Jeon, T. W. Kang, R. Singh, K. Sharma, and R. K. Choubey, "Structural and optical properties of silica capped ZnS: Mn quantum dots," *J Mater Sci: Mater Electron*, vol. **26**, pp. 3939-3946, 2015.

[21] M. Y. Shahid, M. Asghar, H. M. Arbi, M. Zafar, and S. Z. Ilyas, AIP Advances **6**, (2016). "Role of magnesium in ZnS structure: Experimental and theoretical investigation," *AIP Advances*, vol. 6, pp. 025019, 2016

[22] R. Subha, V. Nalla, J. H. Yu, S. W. Jun, K. Shin, T. Hyeon, C. Vijayan, and W. Ji, "Efficient Photoluminescence of Mn^{2+}-Doped ZnS Quantum Dots Excited by Two-Photon Absorption in Near-Infrared Window II," *J. Phys. Chem. C.*, vol. 117, pp. 20905-20911, 2013.

[23] Y. Hu, Z. Wei, B. Wu, B. Shen, Q. Dai, and P. Feng, **"**Photoluminescence of ZnS: Mn quantum dot by hydrothermal method," *AIP Advances*, vol. 8, no. 1, pp. 015014, 2018.

[24] C. Ding, Y. Li, and Y. Qu, "Synthesizing quantum dot with uniform grain diameter distribution in water phase comprises preparing molding board agent and cadmium sulfydryl composite precursor, producing water solution of sodium borohydride, and synthesizing quantum dot," *East China Normal University*, 2010.

[25] V. K. T. and S. L. Belagali, "Synthesis and characterization of Mn: ZnS quantum dots for photovoltaic applications," *Nano-Structures and Nano-Objects*, vol. 14, pp. 118–124, 2018.

[26] Y. F. Zhu *et al.*, "Fabrication and photoelectrochemical properties of ZnS/Au/TiO2 nanotube array films," *Phys. Chem. Chem. Phys.*, vol. 15, no. 11, pp. 4041–4048, 2013.

[27] "$Dmol^3$ from Materials Studio 2017," Dassault Systèmes BIOVIA: San Diego (2017).

[28] W. Koch and M. C. Holthausen, "A Chemist's Guide to Density Functional Theory," 2nd ed. (Wiley-VCH, Weinheim, 2001).

[29] B. Delley, "From molecules to solids with the $DMol^3$ approach," Journal of Chemical Physics, vol. 113, pp. 7756–7764, 2000.

[30] H. Labiadh, K. Lahbib, S. Hidouri, S. Touil, and T. B. Chaabane, "Insight of ZnS nanoparticles contribution in different biological uses," *Asian Pac. J. Trop. Med.*, vol. 9, no. 8, pp. 757–762, 2016.

[31] A. S. Abdel-Bary, D. A Tolan, M. Y. Nassar, T. Taketsugu, and A. El-Nahas, " Chitosan, magnetite, silicon dioxide, and graphene oxide nanocomposites: synthesis characterization, efficiency as cisplatin drug delivery, and DFT calculations, Intern. J. Biolog. Macromolec., vol. 154, pp. 621-633, 2020.

[32] J. Tolia, M. Chakraborty, and Z.V. P Murthy, "Photoluminescence of Photocatalytic Degradaded Malachite Green Dye by using Mn-doped ZnS," vol. 24, pp. 489–495, 2011.

[33] L. B. Chandrasekar, R. Chandramohan, R. Vijayalakshmi, and S. Chandrasekaran, "Preparation and characterization of Mn-doped ZnS nanoparticles," vol. 5, pp. 71- 75, 2015.

[34] K. T. Al.- Rasoul, I. M. Ibrahim, I. M. Ali, and R. M. Al-Haddad, "Synthesis, Structure, And Characterization of Zns Qds And Using It In Photocatalytic Reaction," *Int. J. Sci. Technol. Res.*, vol. 3, no. 5, pp. 213–217, 2014.

[35] V. D. Mote, Y. Purushotham, and B. N. Dole, "Structural, morphological and optical properties of Mn-doped ZnS nanocrystals," *Ceramica*, vol. 59, pp. 395–400, 2013.

[36] C. B., K. R., and B. M. G. Murray, "Synthesis and Characterization of Capped ZnS Quantum Dots," in *Annu. Rev. Mater. Sci.*, vol. 30, pp. 545–610, 2006.

[37] B. Kaur, S. Chand, K. Singh, and A. K. Malik, "Detoxification of dye contaminated water by

Mn^{2+}-doped ZnS nanostructures," *Bull. Mater. Sci.*, vol. 42, no. 2, pp. 1–9, 2019.

[38] X. Chen, W. Liu, G. Zhang, N. Wu, L. Shi, and S. Pan, "Efficient Photoluminescence of Mn^{2+}-Doped ZnS Quantum Dots Sensitized by Hypocrellin A," *Adv. Mater. Sci. Eng.*, vol. 2015, 2015.

[39] I. M. Ali, R. M. Al-Haddad, and K. T. Al-Rasoul, "Structural and Optical Properties of Synthesized Manganese doped ZnS Quantum Dots," *Int. J. Innov. Sci. Eng. Technol.*, vol. 1, no. 10, 2014.

[40] V. K. Gupta, A. Fakhri, M. Azad, and S. Agarwal, "Synthesis and characterization of Ag-doped ZnS quantum dots for enhanced photocatalysis of Strychnine as a poison: Charge transfer behavior study by electrochemical impedance and time-resolved photoluminescence spectroscopy," *J. Colloid Interface Sci.*, vol. 510, pp. 95–102, 2018.

[41] J. P. Borah and K. C. Sarma, "Optical and optoelectronic properties of ZnS nanostructured thin film," *Acta Phys. Pol. A* vol. 114, no. 4, pp. 713–719, 2008.

[42] A. K. Shahi, B. K. Pandey, S. C. Singh, and R. Gopal, "Observation of negative persistent photoconductivity in ZnS/PVA nanocomposite materials," *J. Alloys Compd.*, vol. 588, pp. 440–448, 2014.

[43] K. S. Ojha, "Structural and optical properties of PVA doped zinc sulphide thin films," *Optik (Stuttg).*, vol. 127, no. 5, pp. 2586–2589, 2016.

[44] J. Alin, M. Rubino, and R. Auras, "Effect of the Solvent on the Size of Clay Nanoparticles in Solution as Determined Using an Ultraviolet-Visible (UV-Vis) Spectroscopy Methodology," *Appl. Spectrosc.*, vol. 69, no. 6, pp. 671–678, 2015.

[45] A. B. Cruz, Q. Shen, and T. Toyoda, "The effect of ultraviolet irradiation on the photothermal, photoluminescence and photoluminescence excitation spectra of Mn-doped ZnS nanoparticles," *Thin Solid Films*, vol. 499, pp. 104–109, 2006.

[46] Y. S. Lim, C. K. Lo, and G. B. Teh, "Unsaturated polyester resin blended with MMA as potential host matrix for luminescent solar concentrator," *Renew. Energy*, vol. 45, pp. 156–162, 2012.

[47] C. Carrillo-Carrión, S. Cárdenas, B. M. Simonet, and M. Valcárcel, "Quantum dots luminescence enhancement due to illumination with UV/Vis light," *Chem. Commun.*, no. 35, pp. 5214–5226, 2009.

[48] Y. F. Zhu *et al.*, "Fabrication and photoelectrochemical properties of ZnS/Au/TiO2 nanotube array films," *Phys. Chem. Chem. Phys.*, vol. 15, no. 11, pp. 4041–4048, 2013.

[49] B. Ayim-Otu, M. Kuncan, Ö. Şahin, and S. Horoz, "Synthesis and photovoltaic application of ZnS: Cu (3%) nanoparticles," *J. Aust. Ceram. Soc.*, vol. 56, no. 2, pp. 639–643, 2020.